HHS Public Access

Author manuscript

Biomed Mater. Author manuscript; available in PMC 2018 December 28.

Published in final edited form as:

Biomed Mater. ; 13(1): 015023. doi:10.1088/1748-605X/aa895c.

Cell Derived Extracellular Matrix Fibers Synthesized Using Sacrificial Hollow Fiber Membranes

Kevin Roberts[a], **Jacob Schluns**[b], **Addison Walker**[b], **Jake D. Jones**[b], **Kyle P. Quinn**[b], **Jamie Hestekin**[c], and **Jeffrey C Wolchok**[b,*]

[a]Cell and Molecular Biology Program, University of Arkansas, 850 W. Dickson St. Rm. 601, Fayetteville, Arkansas 72701

[b]Department of Biomedical Engineering, University of Arkansas, 790 W. Dickson St. Rm. 120, Fayetteville, Arkansas 72701

[c]Ralph E. Martin Department of Chemical Engineering, University of Arkansas, 800 W. Dickson St. Rm. 3202, Fayetteville, Arkansas 72701

Abstract

The therapeutic potential of biological scaffolds as adjuncts to synthetic polymers motivates the engineering of fibers formed using the extracellular matrix (ECM) secreted by cells. To capture the ECM secreted by cells during *in vitro* culture, a solvent degradable hollow fiber membrane (HFM) was created and utilized as a cell culture platform. NIH/3T3 fibroblasts were injected into the narrow (0.986 ± 0.042 mm) lumina of mesoporous polysulfone HFMs and maintained in culture for up to three weeks. Following cell culture, HFMs were dissolved using N-methyl-2-pyrrolidone and the accumulated ECM was collected. The ECM retained the filamentous dimensions of the HFM lumen. The process yielded up to 0.89 ± 0.20 mg of ECM for every mm of HFM dissolved. Immunofluorescence, second-harmonic generation microscopy, and tandem mass spectrometry indicated the presence of an array of ECM constituents, including collagen, fibronectin, and proteoglycans, while FTIR spectra suggested thorough HFM material dissolution. Isolated ECM fibers, although fragile, were amenable to handling and exhibited an average elastic modulus of 34.6 ± 15.3 kPa, ultimate tensile strength of 5.2 ± 2.2 kPa, and elongation-at-break of 29% ± 18%. ECM fibers consisted of an interconnected yet porous (32.7% ± 5.8% open space) network which supported the attachment and *in vitro* proliferation of mammalian cells. ECM fibers were similarly synthesized using muscle and astrocyte cells, suggesting process robustness across different cell types. Ultimately, these ECM fibers could be utilized as an alternative to synthetics for the manufacture of woven meshes targeting wound healing or regenerative medicine applications.

[*] *Corresponding author and person to whom reprint requests should be addressed:* Jeffrey C. Wolchok, PhD, Department of Biomedical, Engineering University of Arkansas, John A. White, Jr. Engineering Hall, Suite 120, Fayetteville, Arkansas, Phone: 479-575-4667, jwolchok@uark.edu.

Disclosures

Conflicts of interest: none.

1. Introduction

Woven surgical meshes are extensively utilized for the repair of damaged tissues. Each year over 1 million surgical meshes are implanted worldwide [1]. These meshes are typically fabricated using synthetic polymer fibers, the most common being polypropylene. Biomaterial fibers are highly versatile materials that can be woven into a range of implant geometries (meshes, tubes, ropes) using high throughput fabrication methods developed and routinely used by the textiles industry. However, the dramatic rise in the use of surgical meshes has been matched by a similar rise in serious post-surgical complications and product recalls [2–4]. The complications associated with surgical meshes appear to be a direct consequence of the host response to synthetic polymer implants [5]. Specifically, the aggressive foreign body response, characterized by fibrotic tissue formation combined with the chronic activation of immune cells at the site of implantation, appears to be a serious roadblock to clinical success [6]. In fact, the aggressive fibrotic response directed against implanted synthetic materials requires that surgical meshes be applied only where scarring at the site of implantation can be tolerated. For instance, in cases where woven meshes are used to repair hernias the dense scarring response strengthens the repair site [7]. However, for many regenerative applications (muscle, vessel, nerve), the restoration of native tissue structure is the goal, and therefore the disorganized scarring associated with the foreign body response is a severe disadvantage. Ultimately, while fibers have tremendous potential as the raw material for biomedical implants, synthetic polymer fibers are unlikely to find clinical utility for the repair of non-connective tissue types. For cardiac, vascular, nervous, and muscle tissue repair, the need exists for a biomaterial fiber that can be remodeled by the body's own wound healing machinery.

Extracellular matrix (ECM) is a network of biomolecules secreted by all somatic cells of the body which functions as both a physical support for tissues and a reservoir of chemical cues which guide cell differentiation, migration, and tissue remodeling [8]. ECM is noted for its regenerative capacity, with several clinical studies having demonstrated the efficacy of ECM-based grafts for repair of heart, skin, cartilage, and other tissues [9–12]. Of particular relevance to woven meshes, published evidence suggests that fibers containing extracellular matrix (ECM) molecules mute the foreign body reaction and enhance regeneration [13, 14]. Specifically, Badylak and colleagues have shown that ECM-coated synthetic meshes reduced the fraction of pro-inflammatory M1 macrophages at the site of implantation and that this change enhanced tissue remodeling. However, while composite ECM/synthetic fibers may delay a foreign body response, they are unlikely to eliminate it completely. As the ECM degrades and the underlying synthetic material interface is exposed to the immune system, a foreign body reaction will eventually be initiated. We suggest that fiber built entirely from ECM -carrying an arsenal of macromolecules relevant to wound-healing-is a logical next step toward the development of whole ECM meshes which may have clinical utility as an adjunct to synthetic polymers.

To create ECM fibers, our group has previously explored methods to farm the ECM secreted by populations of mammalian cells during growth in culture [15, 16]. The creation of ECM fibers is predicated by a simple principle; cells have the ability to produce ECM, and the primary challenge is to develop methods to concentrate and collect the molecules that they

secrete. Toward this end, we have explored a technique to facilitate the accumulation of cell-secreted molecules using hollow fiber membranes (HFMs) as a cell culture platform. When the lumen is seeded with cells, the semipermeable HFMs trap the large cells and secreted ECM molecules, but permit the exchange of smaller cell culture nutrients. The application of HFM's for cell culture is not unique by itself, semipermeable HFM's have been used as platforms for the cultivation, implantation, and immuno-isolation of hepatocytes and pancreatic islet cells [17, 18]. What's unique is the sacrificial role of the HFM. Rather than being a permanent component, it instead serves as a temporary platform used to capture and collect cell secreted ECM. Once sufficient ECM has been collected, the synthetic HFM can be dissolved, leaving behind only the accumulated ECM which retains the shape of the lumen. In this study, we describe this novel scheme for the production of ECM fibers using sacrificial HFMs as a cell culture platform, and present the characterization results for several key ECM fiber physical and chemical properties.

2. Materials and Methods

2.1. Preparation of Hollow Fiber Membranes

Mesoporous polysulfone HFMs were manufactured using a common dry-jet wet spinning method (Table 1) [19]. Polysulfone pellets (35kD, Sigma, St. Louis MO) were dissolved in N-methyl-2-pyrrolidone (NMP, 17.8 w/w%) for three days at 25 °C. Polysulfone (PSF) dope solution and a bore solution of NMP in deionized water (15, w/w%) were extruded through a spinneret (AEI) using pressurized N2. Flow of dope and bore solutions from the spinneret into an air gap and subsequent water bath resulted in precipitation of polysulfone fibers by nonsolvent-induced phase separation (Figure. 1). HFMs were stored in deionized water for three days, with water exchanged once per day for removal of residual solvent.

2.2. Cell Culture

To facilitate cell culture, HFMs were sterilized in 70% ethanol for 24 hours and incubated in a solution of bovine plasma fibronectin (20 μg/mL) at 37 °C for one hour, after which they were cut using sterile scissors to lengths of 6 cm for cell-seeding. Frozen NIH/3T3 fibroblasts (ATCC, Manassas, VA), suspensions were thawed, seeded into T-175 flasks, and cultured until confluent in DMEM/F12 containing 10% (w/v) fetal-bovine serum (FBS), 1% L-glutamine, and 1% penicillin-streptomycin. Confluent cultures were disassociated using 0.25% Trypsin-EDTA prior to centrifugation. Pellets were resuspended in DMEM/F12, with cell density counted using a hemocytometer. Cells were seeded into the lumina of HFMs at a density of approximately 20K cells/cm of fiber length using a sterile 21-gauge needle and syringe.

All cell seeded HFMs were cultured for durations of either one or three weeks in DMEM/F12 supplemented 10% (w/v) FBS, 1% L-glutamine, 1% penicillin-streptomycin, 0.285 mM L-ascorbic acid (Sigma), 0.5 mM L-ascorbic acid 2-phosphate (Sigma), and 5 ng/mL human TGF-β1 (Peprotech, Rocky Hill, NJ). At the completion of the culture period, cell-seeded HFMs were dissolved in 99.5% NMP for three days, with NMP exchanged once per day. The remaining cell-derived material (ECM fiber) was collected, rinsed for 48 hours in DI water, and characterized. A subset of HFMs were seeded and cultivated with rat

astrocyte and skeletal muscle fibroblast cells to evaluate process robustness across cell types. Astrocyte and muscle cells were harvested via methods approved by the University of Arkansas Institutional Animal Care and Use Committee (IACUC).

2.3. Characterization

Transverse cross-sections of naïve polysulfone HFMs were fractured in liquid nitrogen and imaged by SEM to visualize membrane morphology. HFM inner diameter, outer diameter, and wall thickness were measured from microscope images collected from representative samples (n =10). The pore-size distributions of HFMs were determined using evapoporometry and guided by published protocols [20–22]. HFMs were fixed to plastic test cells (n = 3) using an epoxy resin, immersed in 99.5% isopropanol, and mass loss due to evaporation of isopropanol was measured for 24 hours, from which pore-size distributions were calculated using equations described by Krantz *et al.* [22]. Evapoporometry was chosen as the technique for probing pore size in this investigation, as it avoids the application of significant pressure to a sample, is non-destructive, and has been applied successfully toward the analysis of the selective layers of pores between 4 nm to 365 nm in asymmetric membranes, including hollow fiber membranes similar to those produced in this investigation [23, 24].

The effectiveness of the NMP dissolution method was assessed using attenuated total reflectance Fourier transform infrared spectroscopy (ATR-FTIR) with a resolution of 8 cm^{-1} and a scanning range of 900–1800 cm^{-1}. ATR-FTIR spectra for representative NIH/3T3 derived ECM fibers, cultured polysulfone HFMs, and naive HFMs were analyzed for the presence of sulfonyl groups and aromatics characteristic of polysulfone, as well as protein-characteristic amide bands.

In preparation for characterization, NIH/3T3 derived ECM fibers were decellularized using a detergent based protocol [25]. Samples were rinsed for 90 min in Tris-HCL (10mM, pH8.0) with 1% EDTA and 10KU/ml aprotinin 4°C with agitation. Samples were then soaked in 0.1% sodium dodecyl sulphate (SDS) in Tris-HCL buffer for 24 hours at room temperature with agitation. To remove nuclear remnants samples were then incubated for 3 h in reaction buffer containing 50U/mL deoxyribonuclease I and 1U/mL ribonuclease A in 10mM Tris-HCl (pH 7.5) at 37°C with agitation. To assess decellularization effectiveness, treated and control samples (n=3/sample group) were fluorescently stained for the presence of the cytoskeletal protein actin using phalloidin (1:40, Sigma). Cells were counterstained with the nuclear reagent DAPI. Representative decellularized material samples were imaged for comparison to cell-containing controls.

Decellularized NIH/3T3 derived ECM fibers were rinsed in deionized water and weighed. Yields were calculated relative to HFM length (mg/mm). Astrocyte and muscle cell derived ECM fiber yield was similarly measured. To examine the internal structure, hydrated NIH/3T3 ECM fiber samples (n=3) were sectioned (7 μm) with the aid of a cryostat (Leica), mounted onto microscopic slides, stained with hematoxylin and eosin and imaged. From the digital images, the porosity (% open area) was calculated from transverse ECM fiber sections with the aid of image analysis software (ImageJ), through subtraction of freehand-bounded pore area from total section area and dividing the difference by total section area to

yield porosity. To visualize fiber surface features, NIH/3T3 derived fiber samples were frozen, lyophilized, and imaged using scanning electron microscopy (SEM). The SEM imaging of lyophilized samples was motivated by the anticipated use of freeze-drying to prepare materials for storage and implantation.

HFM and decellularized NIH/3T3 ECM fiber mechanical properties were measured with the aid of a uni- axial mechanical testing device (5994, Instron, Norwood, MA) using techniques familiar to our group [16, 26, 27]. Hydrated (PBS, pH = 7.4) samples (gauge length = 1 cm) were deformed at a constant strain rate of 10%/min until failure using a 1N load cell while load and displacement values were recorded at 10 Hz. Prior to testing, sample (n = 4/sample group) fiber diameter was measured using digital calipers. For each sample, engineering stress versus strain curves were generated from load and elongation data. Strain was determined using grip displacement values. From each curve, the tangent modulus was calculated using a linear fit to the region of the stress-strain curve extending from the end of the toe in region, approximately 10% and 0.5% strain for ECM and HFM fibers respectively, to the point of sample failure. The ultimate strength was calculated as the peak stress achieved by each fiber prior to failure.

NIH/3T3 ECM fibers were assessed for the presence of accumulated ECM constituent proteins by immunofluorescence. Representative fibers were immunoreacted for the presence of cellular fibronectin (Mouse IgM, 1:500, Sigma) followed by the appropriate fluorescently labeled secondaries (1:500, Alexafluor, Life Technologies). Samples were counterstained with the nuclear staining reagent DAPI, and then microscopically imaged using an Eclipse Ci-S microscope with D-FL epifluorescence attachment (Nikon, Tokyo, Japan). The accumulation of organized fibrillary collagen within ECM fiber samples was assessed using label free second harmonic generation microscopy (Ultima Investigator, Bruker Inc., Middleton, WI) [25].

NIH/3T3 ECM fiber proteomic composition was further assessed using tandem mass spectrometry (MS/MS). MS/MS was performed with the aid of the University of Arkansas for Medical Sciences proteomics core facility. Samples were hydrated in acetonitrile, digested with trypsin in 100 mM ammonium bicarbonate at 37°C for 12–16 hours. Tryptic peptides were separated by reverse phase Jupiter Proteo resin (Phenomenex) on a 200 × 0.075 mm column using a nanoAcquity UPLC system (Waters). Eluted peptides were ionized by electrospray (2.15kV) followed by MS/MS analysis using higher-energy collisional dissociation (HCD) on an Orbitrap Fusion Tribrid mass spectrometer (Thermo Scientific, Waltham, MA) in top-speed data-dependent mode. Proteins were identified by comparison to a proteomics database (Mascot, Matrix Science). Scaffold proteomics software was used to verify MS/MS protein identification, with identifications accepted if established with a less than 1% false discovery rate as determined by Scaffold's local FDR algorithm.

A direct contact assay was employed to assess cellular attachment and proliferation upon ECM fiber materials. In preparation for cytotoxicity assays, decellularized NIH/3T3 ECM fibers (approximate length = 1cm) and unmodified glass coverslips (n = 3/sample group) were sterilized for 24 hours in 70% ethanol. NIH/3T3 cells were seeded onto each sample at

a density of 10 K cells per sample, and cultured in DMEM-F12 with 10% (w/v) FBS, 1% L-glutamine, and 1% penicillin-streptomycin. Following 72 hours of culture, samples were assayed for cell viability and death via Calcein AM (2 μM in PBS) and EthD-1 (4μM in PBS), respectively. Calcein stained ECM fibers were microscopically imaged and assessed for cell coverage.

In-vivo host response was examined using a subcutaneous implant site. *In-vivo* biocompatibility was assayed at 2 and 6 weeks post-implantation time points. Mature male Sprague Dawley rats (300+g) were used (Envigo, IN). All surgical procedures were performed in accordance with protocols approved by the University of Arkansas Institutional Animal Care and Use Committee. Anesthesia was induced using isoflurane (2–4%) in oxygen. The subcutaneous implant site was surgically exposed through a 2 cm left-right incision placed caudal to the scapulae. A subcutaneous pouch was created in each animal by blunt dissection. A single NIH/3T3 ECM sample was implanted into each pouch (approximate implant size 10mm diameter). Incisions were closed using surgical adhesive (VetBond, 3M). Following surgery all animals were housed in the University of Arkansas Central Laboratory Animal Facility. At the prescribed time-points all animals (n=3/timepoint) were euthanized via inhalation of carbon dioxide. The implant site with surrounding soft tissue was harvested, fixed in 4% paraformaldehyde, paraffin embedded, sectioned (10um), and stained with H&E. Stained sections were imaged and examined for evidence of inflammation and material degradation.

2.4 Statistical Methods

All data are represented as mean and standard deviation. The effect of cell type and culture duration on ECM fiber yield was evaluated with a two-way ANOVA with interaction term. Post hoc comparisons were made using Tukey's test. A standard 0.05 level of significance was used for all statistical tests.

3. Results

Hollow fiber membranes (HFMs) fabricated by the dry-jet wet spinning technique (Fig. 1) were of the asymmetric type, with selective inner and outer skin layers supported by a highly porous intermediate layer (Figure. 2). Approximately 100 meters of HFM were fabricated from 300 mL of 17.8 w/w% polysulfone in N-methyl-2-pyrrolidone. Evapoporometry analysis of the HFMs revealed a mesoporous pore size distribution, with an average pore diameter of 39.8 nm ± 3.9 nm. HFM geometry was consistent both within and between batches, with average inner and outer diameters of 0.986 mm ± 0.042 mm and 1.29 mm ± 0.038 mm, respectively.

Material harvested from HFMs cultured with NIH/3T3 fibroblasts, rat skeletal muscle fibroblasts (RSMF), and astrocytes was translucent, showed no visual evidence of residual HFM, and exhibited a continuous filament geometry similar to the diameter and length of the HFMs in which they were cultured (Figure. 3). Fibers were amenable to handling and could be woven into a simple crosshatch pattern in a manner consistent with traditional fiber weaving techniques. HFMs cultured with NIH/3T3 cells for three weeks yielded just under one milligram (0.89 ± 0.2 mg/mm) of ECM fiber for every mm of HFM seeded. Although

still capable of producing continuous fibers, both skeletal muscle fibroblasts and astrocyte cells yielded significantly less ECM fiber material (0.44± 0.08 and 0.41± 0.04 mg/mm respectively). ECM fiber yield was sensitive to culture duration. 3T3 cells exhibited a 4- fold increase in ECM yield for three weeks versus one week of culture ($p = 0.0134$). Corresponding increases in yield for skeletal muscle fibroblasts and astrocytes were 2- fold ($p = 0.6965$) and 4-fold ($p= 0.5316$), respectively.

Transverse and longitudinal sections of NIH/3T3 ECM fibers (7 μm thickness) revealed a porous yet interconnected network of eosin stained ECM (Figure. 4). ECM fibers exhibited open-cell pores distributed irregularly throughout the sections. Analysis of transverse sections indicated an average interior ECM fiber porosity of 32.7% ± 5.8%. SEM images of lyophilized NIH/3T3 ECM fibers revealed a dense surface skin with a rough filamentous texture that is consistent with the appearance of native tissue ECM. The surface skin also showed evidence of fibril alignment along the longitudinal axis of the ECM fiber. Residual HFM material was not observed.

ATR-FTIR spectra of NIH/3T3 ECM fibers revealed strong absorbance at 1650 cm^{-1} and 1540 cm^{-1}, consistent with the amide I and II absorbance bands characteristic of proteins (Figure 5) [28]. Comparison of the spectra of isolated ECM fibers to the spectra of cultured and uncultured polysulfone HFMs indicated that the characteristic polysulfone absorbance peaks (1580, 1480, 1236, and 1150 cm^{-1}) were not present in the ECM fiber samples, suggesting effective dissolution of the polysulfone HFM via NMP incubation.

Mechanical testing of HFMs (Figure 6) yielded an average elastic modulus of 10.0 MPa ± 1.82 MPa and an average ultimate strength of 0.717 MPa ± 0.124 MPa. Stress-strain curves for HFMs exhibited linear elastic regions followed by small plastic regions and sharp failure. HFMs stretched to an average of strain of 13% prior to failure. Stress-strain curves for decellularized NIH/3T3 ECM fibers consistently exhibited toe-in regions, typically extending out to 10%, followed by a near linear increase in stress until failure. No significant plastic region was observed. The average elastic modulus and ultimate strength for ECM fibers measured within the linear region were 34.6 ± 15.3 kPa and 5.2 ± 2.2 kPa respectively. On average, ECM fibers stretched 29% ± 18% in length before failure. The accumulated ECM fibers were notably less stiff and more extensible than the once present HFM scaffolds.

Isolated NIH/3T3 ECM fibers were strongly reactive to antibodies directed against fibronectin (Figure 7). Second harmonic generation imaging also indicated the presence of fibrillary collagen throughout the ECM fibers. MS/MS proteomic analysis identified an array of ECM structural components (Table 2), including collagen I, III, VI, XVIII, fibronectin, fibrillin 1, fibulin 1 and 2, and prolargin. Several matricellular proteins were also present, including EFEMP 1 and 2, thrombospondin 1 and 2, tenascin, and periostin. A complement of proteoglycans was identified as well, including biglycan, decorin, glypican 1 and 6, and versican. Pre-decellularization samples were strongly reactive to phalloidin and DAPI staining, while post-decellularization samples exhibited no specific staining. The gross appearance and handling of ECM fibers was not significantly altered by decellularization, as fibers remained continuous and amenable to handling.

When reseeded with cells, the NIH/3T3 ECM fibers supported the attachment and re-cultivation of NIH/3T3 fibroblasts. Calcein AM staining directed against NIH/3T3 cells indicated that viable cells were distributed densely across the surface of the cultured fibers, reaching confluency within 72 hours (Figure 8). EthD-1 staining indicated a negligible quantity of non-viable cells. No pre-culture treatments (e.g. incubation with fibronectin) were required for adhesion of cells to the ECM fibers.

All implanted animals tolerated the implantation surgery well and gained weight throughout the observation period at a rate (8±2 grams/week) that was not significantly different from un-implanted controls (9±2 grams/week). At 2 weeks post implantation, samples were well incorporated into the surrounding tissue and host cells had densely penetrated the material (Figure 8). There was no evidence of a dense fibrous encapsulation layer surrounding the implants, nor a necrotic region within it. By 6 weeks post implantation, implant sites showed evidence of elevated cellularity, but it was sharply reduced when compared to 2 week samples, suggesting ongoing implant degradation. There was no evidence of local toxicity nor was there any evidence of multinuclear giant cell formation in regions surrounding the implants at either timepoint.

4. Discussion

In this study, we have developed a process for extracting whole threads of ECM secreted by cells cultured in the lumina of sacrificial HFMs. Our findings suggest that this HFM culture approach is amenable toward the production of filaments of ECM from several cell types, and that these filaments have a composition and structure that may find utility for the repair of fibrous tissues in the form of a surgical mesh. The operating principle of the sacrificial HFM culture method is that ECM produced by cells cultured in the lumina of HFM's can be captured and concentrated by preventing cross-membrane transport of ECM constituents. To our knowledge, this study represents the first time in literature that culture of cells in the lumen of HFMs has been leveraged for the production and extraction of ECM. Evapoporometry data indicate that the pores of the membranes fabricated in this study are substantially smaller than the hydrodynamic radii for ECM components such as collagen I (>80 nm at 37 °C) [29, 30] or high molecular weight hyaluronan (103 nm for mW = 2000 kDa) [31], indicating that these constituents are unlikely to diffuse across the membrane, driving ECM to accumulate in the lumina of the HFMs. Conversely, the small hydrodynamic radii of cell medium constituents such as bovine serum albumin (3.48 nm) [32] suggests that they can diffuse across the membrane wall unimpeded. While an in-depth study of ECM bioseparation was beyond the scope of this investigation, the pore diameter distributions of HFMs, being tunable during the spinning process, may allow for selective retention of desirable ECM constituents such as high molecular weight hyaluronan (anti-inflammatory) while permeating others (e.g., pro-inflammatory low mW hyaluronan) [33]

Incorporation of ECM components into a fiber geometry is not entirely without precedent. Alberti and Xu used sheets of decellularized tendon to form fiber-like collagen constructs [34]; another notable advance was made by Onoe *et al*, wherein hydrogels treated with individual ECM proteins were seeded with various cell lines to generate long fibers with encapsulated cells [35]; however, the scaffolding material, being composed of a hydrogel

treated with individual ECM proteins, does not approximate the multimolecular nature of ECM. Past investigations have demonstrated that subtle aspects of ECM composition play an important role in tissue regeneration. For example, heparan sulfate proteoglycans (HSPGs) are known to be necessary for FGF-2 signaling which regulates angiogenesis and the proliferation of satellite cells during myogenesis [36] Further, the combination of glycosaminoglycans and structural proteins in biomaterials have been shown to improve primary muscle cell proliferation, myoblast fusion, and skin regeneration, as well as bone formation *in vivo* [37–40]. The literature at large therefore suggests that the inclusion of an array of key ECM constituents in scaffolds bears clinical relevance for the regeneration of a range of tissues.

Our data suggest that the ECM fibers isolated in this study are bio-complex; immunoreaction of ECM fibers with antibodies for key ECM constituents, second-harmonic generation microscopy, and tandem mass spectrometry appear to demonstrate the multimolecular nature of this material. Several of the ECM constituents identified in ECM fibers are critical elements for the regeneration of a broad range of tissues including skeletal muscle, a target of interest for our group [41]. The fibril- forming collagens I and III found in ECM fibers are the predominant collagens in skin tendon, bone, and skeletal muscle, and collagen VI is an important component of the basement membrane surrounding skeletal muscle [42]. Biglycan and decorin, implicated in cutaneous wound healing and key regulators of collagen organization in skeletal muscle-were also identified [43, 44]. Further, some notable secreted factors were present in ECM fibers, including HDGF, IGF-II, and PEDF, playing various roles in liver, bone, and peripheral nerve regeneration [45–48]. While detergent-based decellularization techniques tend to remove various elements of ECM scaffolds, an array of alternative methods exist which may better preserve glycosaminoglycan and growth factor content [49].

Delivery of therapeutic cells for wound-healing, especially progenitor cells, shows unique promise, as their inclusion into implants can promote angiogenesis [50] and diminish the foreign body response to a biomaterial through the downregulation of pro-inflammatory cytokine expression [51]. This, however, presents challenges to scaffold design; the scaffold must obviously exhibit minimum cytotoxicity, but also have properties that serve to retain the desired phenotype of the carried cells, as the absence of cues provided in cell culture may cause them to lose desired characteristics *in vivo.* It has been observed that cells cultured on substrates coated with tissue-specific ECM better retain their differentiated phenotypes, and that progenitor cells exhibit improved proliferation and retention of differentiation potential on these materials [52, 53]. This suggests that scaffolds composed of whole ECM may find applicability as carriers of therapeutic cells. Although cytocompatibility was not examined with progenitor cells, the ECM fibers produced in this study contain key cell attachment proteins and were supportive of NIH/3T3 cell cultivation, with rapid proliferation leading to confluency in 72 hours and negligible cell death. When taken as a whole, the ECM fibers appear to have desirable cell adhesive properties that could be leveraged to deliver a range of attachment dependent cells. Furthermore, while NMP has known systemic and local toxicity at low concentrations [54, 55], the in-vivo and in-vitro biocompatibility testing results indicate that the solvent can be washed from the ECM samples prior to implantation.

One of the recognized limitations of first generation ECM fibers is their modest yield and strength when compared to both synthetic polymers and native tissue ECM. To address this shortcoming, next generation fabrication approaches could draw from the rich repertoire of cell culture techniques known to influence *in vitro* ECM production. Among these, media supplementation with cytokines possessing known ECM stimulatory properties would appear to be a logical first approach. HFM's can be designed with pore diameters that allow the transport of cytokines including, HGF, VEGF, and CTGF into the lumen, while still trapping the larger structural proteins of interest. In addition to cytokines, the addition of crowding-inducing compounds such as dextran sulfate or Ficoll in culture medium has previously been exploited to increase *in vitro* ECM deposition and organization and may provide a unique synthetic approach toward enhancement of ECM fiber yield [56, 57]. Alternatively the cell itself could be manipulated to modulate ECM production. Recently developed CRISPR/Cas9 gene editing techniques [58, 59] may provide a pathway for the production of "designer" cells with targeted ECM production capabilities. For example, the removal of collagen type I genes may create a cell with enhanced collagen type III production. Similar "knock in" gene editing techniques could be used to selectively increase ECM production [60].

In addition to their use in woven implants, ECM fibers could potentially find utility as the print material in 3-D bio-printing systems [61, 62]. The most common type of printing method, fused deposition, utilizes long filaments to build up an object of interest. We could envision a system in which the synthetic fibers are replaced by ECM fibers, which are then used to print organs and tissues. Furthermore, similar in concept to the various synthetic polymer chemistries available with traditional 3-D printing systems, it may be possible to print using an assortment of ECM fibers synthesized using vascular, nerve, and cardiac cells. The data presented in this study demonstrate that ECM fibers are producible across several cell types, including 3T3 fibroblasts, rat skeletal muscle fibroblasts, and astrocytes. While differences in ECM fiber composition between each of these cell types were not explored, it is known that the in-vitro production of ECM does vary by cell types. Variations in ECM production between cell types could be exploited to create a pallet ECM fibers with varying compositions. Using such a system, it may be possible to bio-print tissues and organs with heterogeneous structures and compositions (e.g. vascular fibers embedded within dermal fibers). A further benefit of this platform is that human cells could be leveraged for the production of allogeneic grafts while autologous implants could be produced by isolating and culturing the patient's own cells. While impractical for the rapid treatment of acute injuries, patient specific implants may be applicable for the treatment of chronic injuries.

5. Conclusions

The results of this study suggest that:

1. Hollow fiber membrane cell culture is applicable toward the production of continuous threads of ECM.
2. ECM fibers are amenable to handling and can be assembled into multi-fiber meshes.

3. Isolated ECM fibers exhibit a diverse complement of fibrous ECM proteins, proteoglycans, and matricellular factors.
4. ECM fibers support the in-vitro cultivation of fibroblasts and are well tolerated by the host following implantation.

Acknowledgments

Research reported in this publication was supported by the US National Science Foundation (CMMI-1404716), the National Institute of Arthritis and Musculoskeletal and Skin Diseases of the National Institutes of Health (R15AR064481) as well as the Arkansas Biosciences Institute.

References

1. Cobb WS, Kercher KW, Heniford BT. The argument for lightweight polypropylene mesh in hernia repair. Surg Innov. 2005; 12:63–9. [PubMed: 15846448]
2. Lee D, et al. Transvaginal mesh kits–how “serious” are the complications and are they reversible? Urology. 2013; 81:43–8. [PubMed: 23200966]
3. Nosti PA, Iglesia CB. Medicolegal issues surrounding devices and mesh for surgical treatment of prolapse and incontinence. Clin Obstet Gynecol. 2013; 56:221–8. [PubMed: 23563873]
4. Unger CA, Barber MD. Vaginal Mesh in Pelvic Reconstructive Surgery: Controversies, Current Use, and Complications. Clin Obstet Gynecol. 2015; 58:740–53. [PubMed: 26512439]
5. Klinge U, et al. Foreign body reaction to meshes used for the repair of abdominal wall hernias. Eur J Surg. 1999; 165:665–73. [PubMed: 10452261]
6. Williams DF. On the mechanisms of biocompatibility. Biomaterials. 2008; 29:2941–53. [PubMed: 18440630]
7. Ibrahim AM, et al. Properties of meshes used in hernia repair: a comprehensive review of synthetic and biologic meshes. J Reconstr Microsurg. 2015; 31:83–94. [PubMed: 25192272]
8. Swinehart IT, Badylak SF. Extracellular matrix bioscaffolds in tissue remodeling and morphogenesis. Developmental Dynamics. 2016; 245:351–360. [PubMed: 26699796]
9. Barber FA, et al. A Prospective, Randomized Evaluation of Acellular Human Dermal Matrix Augmentation for Arthroscopic Rotator Cuff Repair. Arthroscopy: The Journal of Arthroscopic & Related Surgery. 2012; 28:8–15. [PubMed: 21978432]
10. Holubec T, et al. The Use of Extracellular Matrix Patches in Cardiac Surgery. Journal of Cardiac Surgery. 2015; 30:145–148. [PubMed: 25533356]
11. Juhasz I, et al. Long-Term Followup of Dermal Substitution with Acellular Dermal Implant in Burns and Postburn Scar Corrections. Dermatology Research and Practice. 2010; 2010:7.
12. Mostow EN, et al. Effectiveness of an extracellular matrix graft (OASIS Wound Matrix) in the treatment of chronic leg ulcers: a randomized clinical trial. J Vasc Surg. 2005; 41:837–43. [PubMed: 15886669]
13. Faulk DM, et al. ECM hydrogel coating mitigates the chronic inflammatory response to polypropylene mesh. Biomaterials. 2014; 35:8585–95. [PubMed: 25043571]
14. Wolf MT, et al. Macrophage polarization in response to ECM coated polypropylene mesh. Biomaterials. 2014; 35:6838–49. [PubMed: 24856104]
15. Hurd SA, et al. Development of a biological scaffold engineered using the extracellular matrix secreted by skeletal muscle cells. Biomaterials. 2015; 49:9–17. [PubMed: 25725550]
16. Wolchok JC, Tresco PA. The isolation of cell derived extracellular matrix constructs using sacrificial open-cell foams. Biomaterials. 2010; 31:9595–9603. [PubMed: 20950855]
17. Ahmed HMM, et al. 3D liver membrane system by co-culturing human hepatocytes, sinusoidal endothelial and stellate cells. Biofabrication. 2017; 9:025022. [PubMed: 28548045]
18. Teotia RS, et al. Islet encapsulated implantable composite hollow fiber membrane based device: A bioartificial pancreas. Mater Sci Eng C Mater Biol Appl. 2017; 77:857–866. [PubMed: 28532102]
19. Wang, LK., et al. Membrane and Desalination Technologies. Humana Press; 2010.

20. Akhondi E, et al. Evapoporometry determination of pore-size distribution and pore fouling of hollow fiber membranes. Journal of Membrane Science. 2014; 470:334–345.
21. Akhondi E, et al. Improved design and protocol for evapoporometry determination of the pore-size distribution. Journal of Membrane Science. 2015; 496:334–343.
22. Krantz WB, et al. Evapoporometry: A novel technique for determining the pore-size distribution of membranes. Journal of Membrane Science. 2013; 438:153–166.
23. Zamani F, et al. Evapoporometry adaptation to determine the lumen-side pore-size distribution (PSD) of hollow fiber and tubular membranes. Journal of Membrane Science. 2017; 526:1–8.
24. Zamani F, et al. Extending the uppermost pore diameter measureable via Evapoporometry. Journal of Membrane Science. 2017; 524:637–643.
25. Mirsadraee S, et al. Development and characterization of an acellular human pericardial matrix for tissue engineering. Tissue Eng. 2006; 12:763–73. [PubMed: 16674290]
26. Lasher RA, et al. Design and characterization of a modified T-flask bioreactor for continuous monitoring of engineered tissue stiffness. Biotechnol Prog. 2010; 26:857–64. [PubMed: 20187075]
27. Wolchok JC, et al. The effect of bioreactor induced vibrational stimulation on extracellular matrix production from human derived fibroblasts. Biomaterials. 2009; 30:327–35. [PubMed: 18937972]
28. Kong J, Yu S. Fourier transform infrared spectroscopic analysis of protein secondary structures. Acta biochimica et biophysica Sinica. 2007; 39:549–559. [PubMed: 17687489]
29. Liu Y, et al. Double thermal transitions of type I collagen in acidic solution. J Biomol Struct Dyn. 2013; 31:862–73. [PubMed: 22963008]
30. Mu C, et al. Temperature induced denaturation of collagen in acidic solution. Biopolymers. 2007; 86:282–287. [PubMed: 17431891]
31. Coleman PJ, et al. Role of hyaluronan chain length in buffering interstitial flow across synovium in rabbits. The Journal of Physiology. 2000; 526:425–434. [PubMed: 10896731]
32. Axelsson I. Characterization of proteins and other macromolecules by agarose gel chromatography. Journal of Chromatography A. 1978; 152:21–32.
33. Petrey AC, de la Motte CA. Hyaluronan, a Crucial Regulator of Inflammation. Frontiers in Immunology. 2014; 5:101. [PubMed: 24653726]
34. Alberti KA, Xu Q. Slicing, stacking and rolling: fabrication of nanostructured collagen constructs from tendon sections. Adv Healthc Mater. 2013; 2:817–21. [PubMed: 23233344]
35. Onoe H, et al. Metre-long cell-laden microfibres exhibit tissue morphologies and functions. Nat Mater. 2013; 12:584–590. [PubMed: 23542870]
36. Yablonka-Reuveni Z, Rivera AJ. Proliferative Dynamics and the Role of FGF2 During Myogenesis of Rat Satellite Cells on Isolated Fibers. Basic and applied myology: BAM. 1997; 7:189–202. [PubMed: 26052220]
37. Rønning SB, et al. The combination of glycosaminoglycans and fibrous proteins improves cell proliferation and early differentiation of bovine primary skeletal muscle cells. Differentiation. 2013; 86:13–22. [PubMed: 23933398]
38. Salbach J, et al. Regenerative potential of glycosaminoglycans for skin and bone. J Mol Med (Berl). 2012; 90:625–35. [PubMed: 22187113]
39. Scuderi N, et al. Clinical application of autologous three-cellular cultured skin substitutes based on esterified hyaluronic acid scaffold: our experience. In Vivo. 2009; 23:991–1003. [PubMed: 20023246]
40. Stadlinger B, et al. Effect of biological implant surface coatings on bone formation, applying collagen, proteoglycans, glycosaminoglycans and growth factors. J Mater Sci Mater Med. 2008; 19:1043–9. [PubMed: 17701311]
41. Ten Broek RW, Grefte S, Von den Hoff JW. Regulatory factors and cell populations involved in skeletal muscle regeneration. J Cell Physiol. 2010; 224:7–16. [PubMed: 20232319]
42. Lampe A, Bushby K. Collagen VI related muscle disorders. Journal of Medical Genetics. 2005; 42:673–685. [PubMed: 16141002]
43. Gillies AR, Lieber RL. Structure and Function of the Skeletal Muscle Extracellular Matrix. Muscle & nerve. 2011; 44:318–331. [PubMed: 21949456]

44. Jarvelainen H, et al. A role for decorin in cutaneous wound healing and angiogenesis. Wound Repair Regen. 2006; 14:443–52. [PubMed: 16939572]
45. Conover CA, et al. Subcutaneous administration of insulin-like growth factor (IGF)-II/IGF binding protein-2 complex stimulates bone formation and prevents loss of bone mineral density in a rat model of disuse osteoporosis. Growth Horm IGF Res. 2002; 12:178–83. [PubMed: 12162999]
46. Enomoto H, et al. Hepatoma-derived growth factor is induced in liver regeneration. Hepatol Res. 2009; 39:988–97. [PubMed: 19624773]
47. Erbay E, et al. IGF-II transcription in skeletal myogenesis is controlled by mTOR and nutrients. The Journal of Cell Biology. 2003; 163:931–936. [PubMed: 14662739]
48. Ho TC, et al. PEDF-derived peptide promotes skeletal muscle regeneration through its mitogenic effect on muscle progenitor cells. Am J Physiol Cell Physiol. 2015; 309:C159–68. [PubMed: 26040897]
49. Gilbert TW, Sellaro TL, Badylak SF. Decellularization of tissues organs. Biomaterials. 2006; 27:3675–3683. [PubMed: 16519932]
50. Leeper NJ, Hunter AL, Cooke JP. Stem Cell Therapy for Vascular Regeneration. Adult, Embryonic, and Induced Pluripotent Stem Cells. 2010; 122:517–526.
51. Swartzlander MD, et al. Immunomodulation by mesenchymal stem cells combats the foreign body response to cell-laden synthetic hydrogels. Biomaterials. 2015; 41:79–88. [PubMed: 25522967]
52. Xiong Y, et al. Retention of the stemness of mouse adipose-derived stem cells by their expansion on human bone marrow stromal cell-derived extracellular matrix. Tissue Eng Part A. 2015; 21:1886–94. [PubMed: 25836590]
53. Zhang Y, et al. Tissue-specific extracellular matrix coatings for the promotion of cell proliferation and maintenance of cell phenotype. Biomaterials. 2009; 30:4021–4028. [PubMed: 19410290]
54. Malek DE, et al. Repeated dose toxicity study (28 days) in rats and mice with N-methylpyrrolidone (NMP). Drug Chem Toxicol. 1997; 20:63–77. [PubMed: 9183563]
55. Solomon HM, et al. 1-Methyl-2-pyrrolidone (NMP): reproductive and developmental toxicity study by inhalation in the rat. Drug Chem Toxicol. 1995; 18:271–93. [PubMed: 8586021]
56. Chen C, et al. Applying macromolecular crowding to enhance extracellular matrix deposition and its remodeling in vitro for tissue engineering and cell-based therapies. Adv Drug Deliv Rev. 2011; 63:277–90. [PubMed: 21392551]
57. Chen CZ, et al. The Scar-in-a-Jar: studying potential antifibrotic compounds from the epigenetic to extracellular level in a single well. Br J Pharmacol. 2009; 158:1196–209. [PubMed: 19785660]
58. Peng Y, et al. Making designer mutants in model organisms. Development. 2014; 141:4042–54. [PubMed: 25336735]
59. Riordan SM, et al. Application of CRISPR/Cas9 for biomedical discoveries. Cell Biosci. 2015; 5:33. [PubMed: 26137216]
60. Wang B, et al. Highly efficient CRISPR/HDR-mediated knock-in for mouse embryonic stem cells and zygotes. Biotechniques. 2015; 59:201–8. [PubMed: 26458548]
61. Chia HN, Wu BM. Recent advances in 3D printing of biomaterials. J Biol Eng. 2015; 9:4. [PubMed: 25866560]
62. Ker ED, et al. Bioprinting of growth factors onto aligned sub-micron fibrous scaffolds for simultaneous control of cell differentiation and alignment. Biomaterials. 2011; 32:8097–107. [PubMed: 21820736]

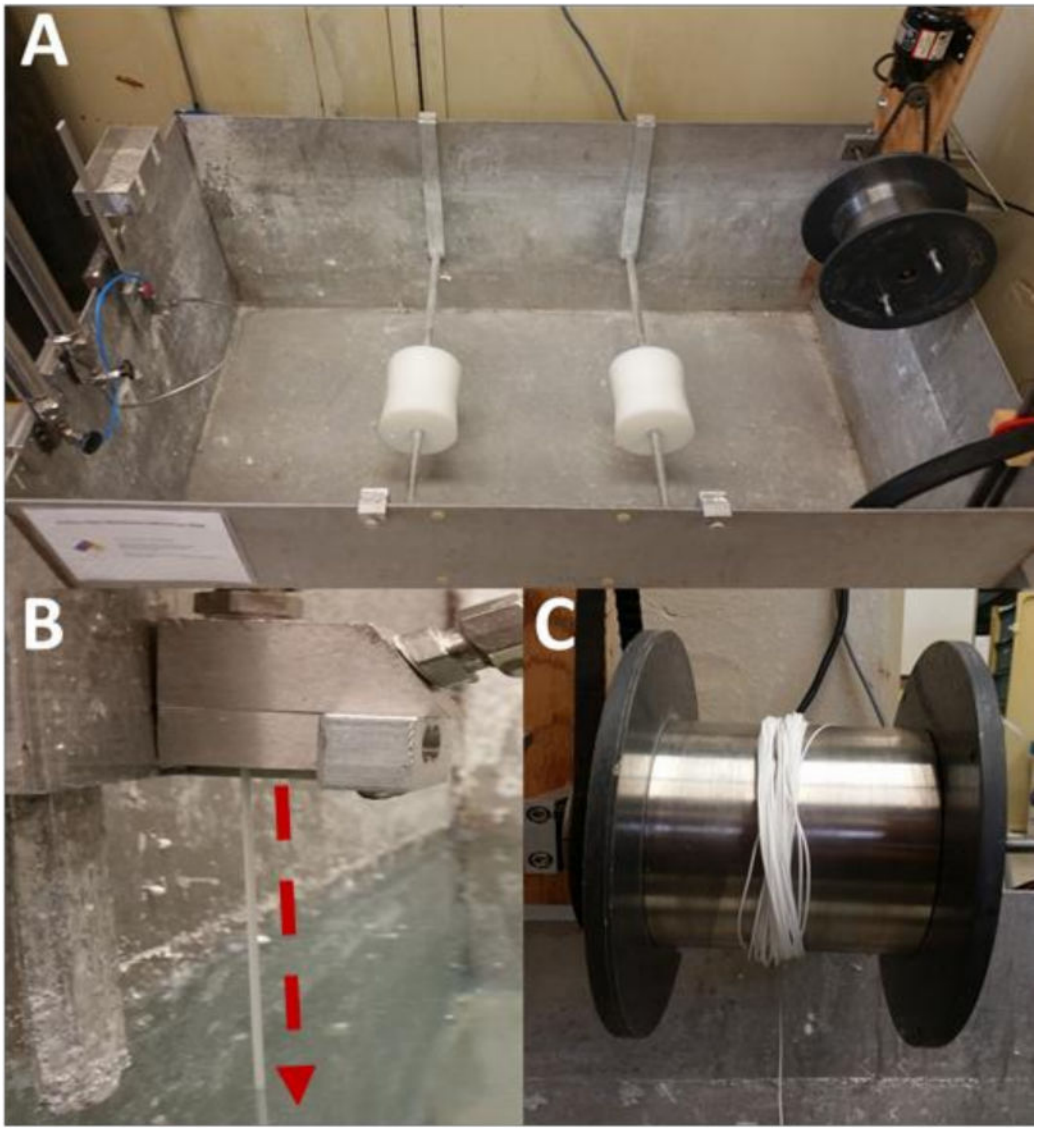

Figure 1. Hollow Fiber Membrane Fabrication

Hollow fiber membranes were fabricated using a custom-built dry-jet wet spinning system (A). Polymer and solvent solutions were extruded by pressurized N_2 through an annulus and needle internal to a spinneret. Solutions exiting the spinneret (B: arrow) begin to form a nascent hollow fiber membrane by non-solvent induced phase separation via contact with the water bath. Following precipitation, membranes were collected on a motorized take-up wheel (C) at a rate of 2.2 meters per minute, producing 100 meters of membrane in 45 minutes.

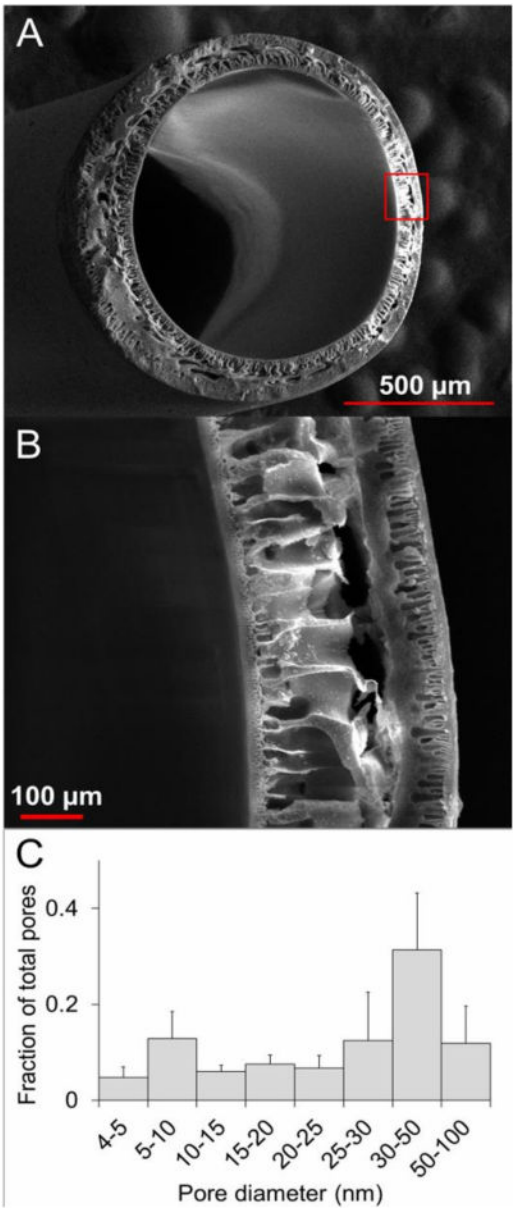

Figure 2. Membrane Structure and Pore Size Distribution

Transverse SEM micrographs (A and B) illustrate the structure of HFM's, which consist of nano-porous interior and exterior skin layers that encapsulate an asymmetric micro-porous (size range 1–500um) interior structural layer. Evapoporometric characterization of the skin layer pore diameter distribution (mean = 39.8 nm ± 3.9 SD, n = 3) revealed a predominantly mesoporous (size range = 1–100nm) distribution of pores with sizes large enough to permit nutrient transport, but small enough to trap large structural proteins within the HFM lumen.

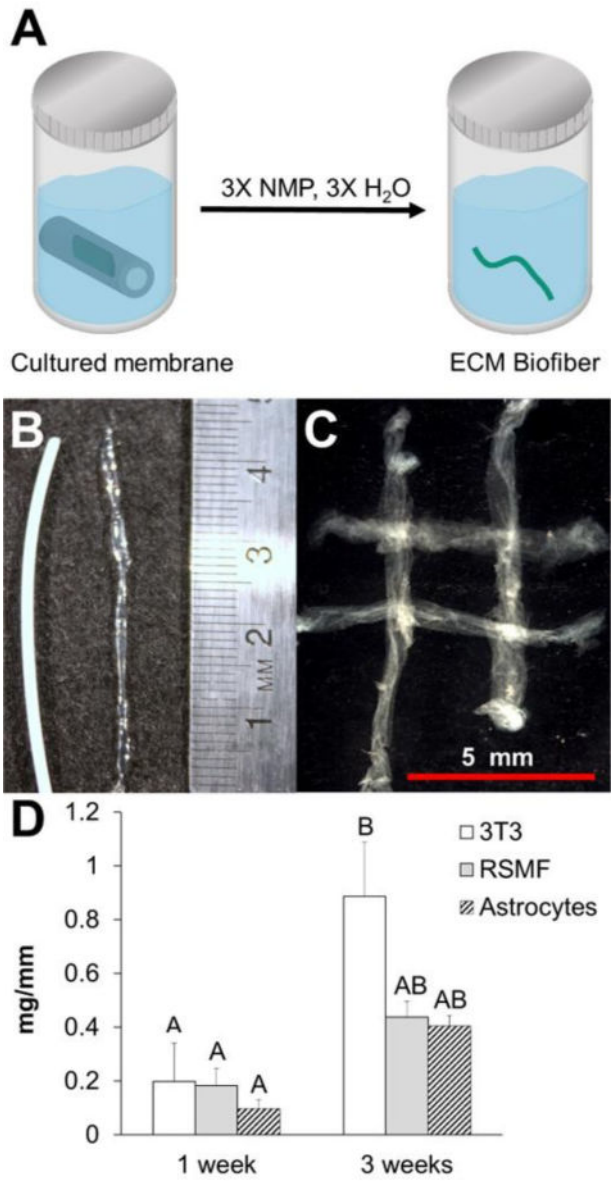

Figure 3. ECM Fiber Collection, Manipulation, and Yield

Following one or three weeks in culture, cell seeded HFMs were (A) dissolved in NMP and the accumulated ECM was collected (green). NIH/3T3 derived material isolated following dissolution (B) retained the filamentous shape of the HFM lumen and could be manipulated into a conceptual weave (C). ECM fibers were similarly synthesized using rat derived astrocytes and skeletal muscle fibroblasts. ECM fiber yield (D) was sensitive to both cell type and culture duration. Levels not connected by same letter are significantly different ($p<0.05$, ANOVA with post hoc Tukey's test).

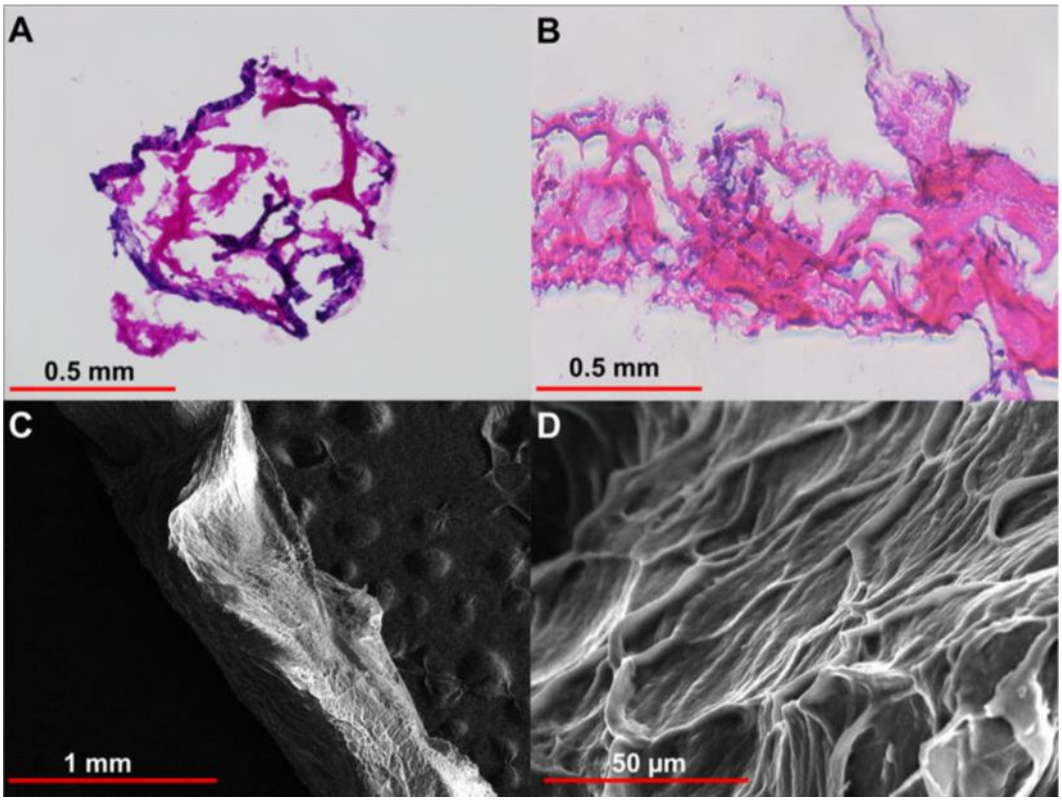

Figure 4. ECM Fiber Structure

Representative H&E stained images of transverse (A) and longitudinal (B) NIH/3T3 ECM fiber thin sections (thickness = 7 μm) illustrates the porous yet interconnect network of accumulated ECM. Transverse sections (n=3) were utilized to quantify fiber porosity. SEM micrographs (C and D) of ECM fibers (50x and 1000x, respectively) illustrate the irregular surface skin with fibrillar features that are suggestive of ECM.

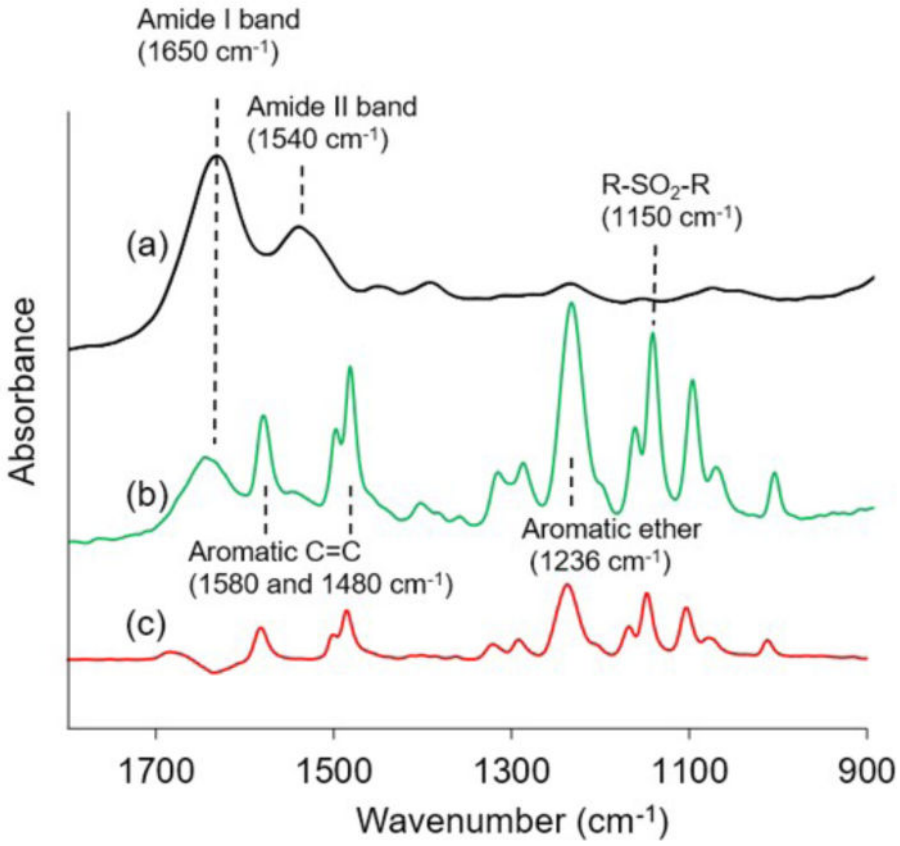

Figure 5. ATR-FTIR Analysis

ATR-FTIR spectra for (a) NIH/3T3-derived ECM fibers, (b) polysulfone HFMs cultured with NIH/3T3 cells for 3 weeks, and (c) uncultured naïve polysulfone HFM were captured using a Spectrum BX FTIR spectrometer with an ATR accessory and a scanning resolution of 8 cm^{-1}. Isolated ECM fibers exhibit strong absorbance in the protein-indicative amide bands, with negligible absorbance for the bands characteristic of polysulfone.

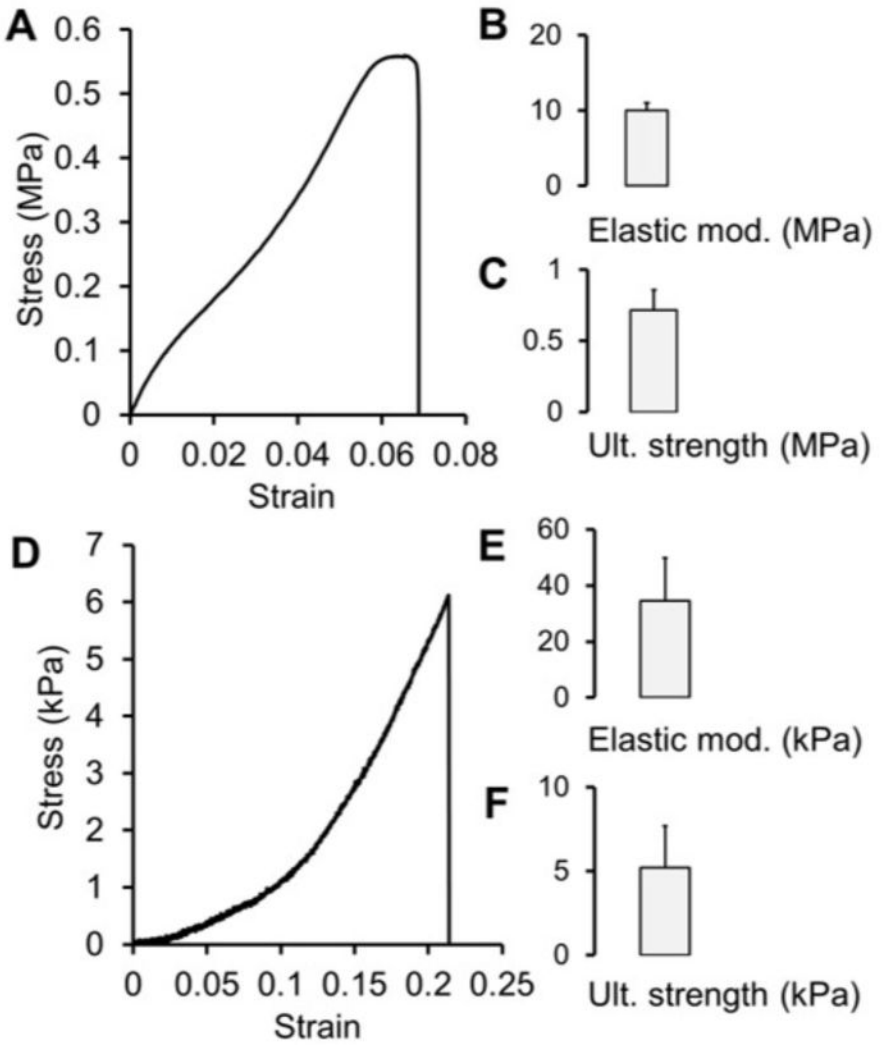

Figure 6. Membrane and ECM Fiber Tensile Properties

Representative HFM stress-strain curve (A), elastic modulus (B) and ultimate strength (C) values for mechanical tested (tensile) HFM samples (mean + SD, n = 3). Representative stress-strain curve (D), elastic modulus (E) and ultimate strength (F) for mechanical tested ECM fibers (mean + SD, n = 3). ECM fiber stress-strain curves were characterized by a toe in region followed by a near linear rise in stress until failure

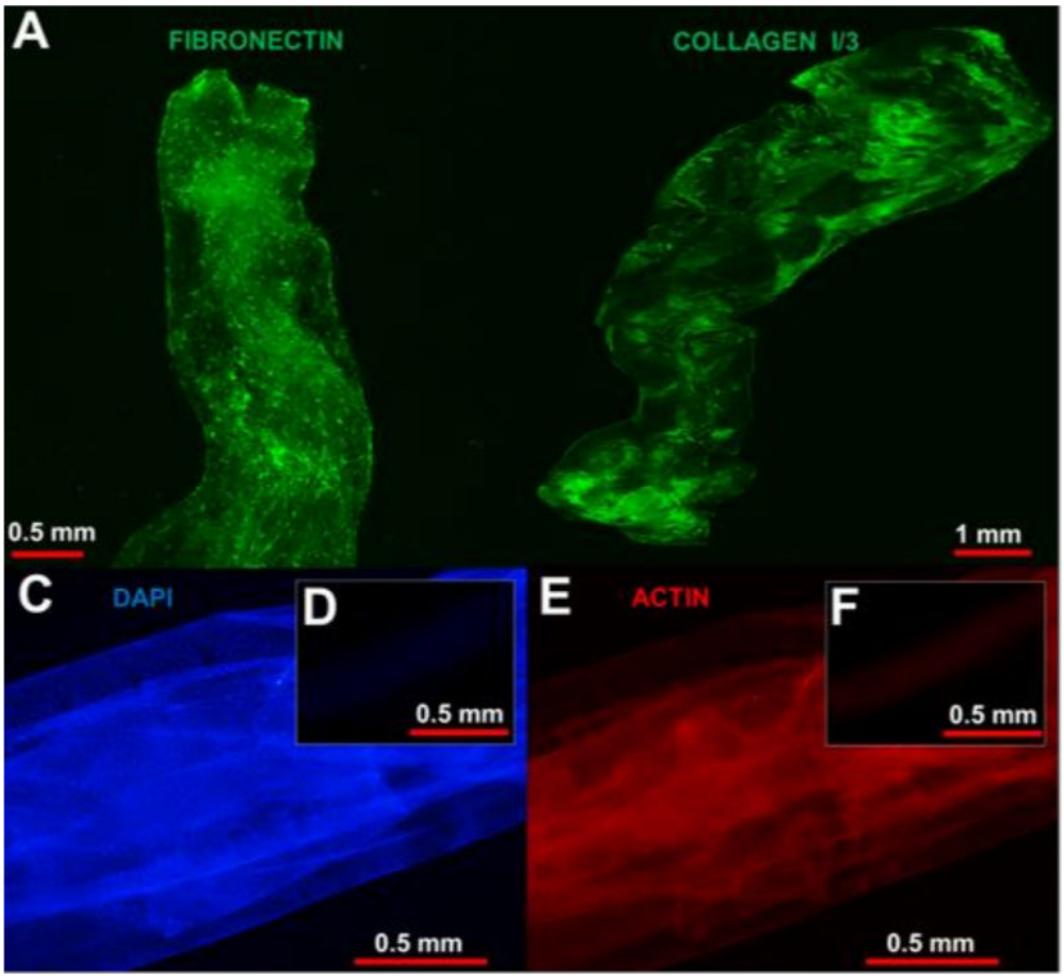

Figure 7. ECM Fiber Immunofluorescence and Decellularization

ECM fibers samples were immuno-stained to detect the presence of fibronectin (A), a key cell adhesive protein. Imaging via second–harmonic generation was utilized to detect the presence of fibrillar collagens, key structural proteins. Prior to decellularization, NIH/3T3 ECM fiber samples (C and E) were strongly reactive to molecules directed against nuclei (blue) and actin (red). Following decellularization (D and F) nuclei and actin could not be detected in any of the samples tested.

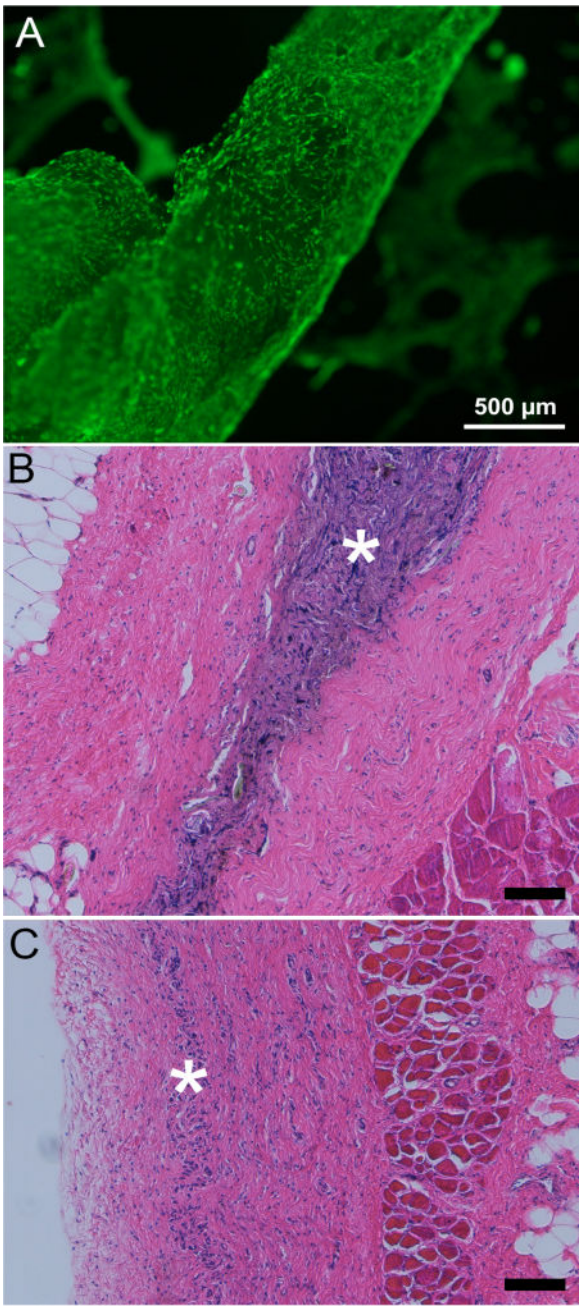

Figure 8. Biocompatibility

Calcein AM cell viability staining of NIH/3T3 fibroblasts seeded and cultured on an isolated ECM fiber for 72 hours (A). Viable cells were attached to and densely distributed across the surface of the ECM fibers. Stained (H&E) thin sections collected from ECM implanted Sprague Dawley rats at 2 (B) and 6 weeks (C), Increased cellularity observed within the dorsal subcutaneous implantation site at 2 weeks (*) is largely resolved by 6 weeks (n=3/ time point). Scale bar 100μm unless noted

Table 1

PSF HFM Spinning Conditions

PSF dope solution (wt.%)	**PSF/NMP (17.8/82.2)**
Bore fluid (wt.%)	NMP/Water (15/85)
Dope extrusion pressure (PSI)	1
Bore extrusion pressure (PSI)	1
Air gap (cm)	8
Take-up speed (m/min)	2.3
External coagulant	Tap water
Coagulant temperature (°C)	24
Dope temperature (°C)	27
Bore temperature (°C)	27
Ambient temperature (°C)	24.6
Humidity (%)	45
Spinneret dimensions (mm)	0.8 I.D./1.6 O.D.

Table 2

ECM Fiber Constituents

Structural and Proteoglycans	Other
Biglycan	EFEMP 1, 2
Collagen I, III, VI, XVIII	EMILIN 1
Decorin	Fibrillin 1
Fibronectin	Fibulin 2, 5
Glypican 1, 6	HDGF
Perlecan	MMP2, 14
Prolargin	PEDF
Versican	Periostin
	Tenascin
	Thrombospondin 1, 2
	TIMP 1, 3